Journal of Power Sources 232 (2013) 264–269

Contents lists available at SciVerse ScienceDirect

Journal of Power Sources

journal homepage: www.elsevier.com/locate/jpowsour

Short communication

Reduction effect of irreversible capacity on SiO anode material heat-reacted with Fe_2O_3

H. Yamamura*, S. Nakanishi, H. Iba

Battery Research Division, Higashifuji Technical Center, Toyota Motor Corporation, 1200 Mishuku, Susono, Shizuoka 410-1193, Japan

HIGHLIGHTS

- The charge–discharge efficiency of high capacity SiO anode material is as low as 75% on first cycle.
- To reduce the oxygen defects in SiO structure, Fe_2O_3 was used as an oxygen source of the redox reaction.
- The charge–discharge efficiency of SiO anode material improves by heat-treated with Fe_2O_3.
- The one of the factor of good reversibility is an improvement of the Li-extraction performance by surface modification.

ARTICLE INFO

Article history:
Received 27 September 2012
Received in revised form
29 November 2012
Accepted 7 January 2013
Available online 16 January 2013

Keywords:
Lithium-ion battery
Anode material
SiO anode
Irreversible capacity
Fe_2O_3

ABSTRACT

Silicon monoxide (SiO) has a high-expected capacity and long cycle performance, but the first cycle's charge–discharge efficiency was lower than that of a conventional anode material. Recently, we have reported that the irreversible capacity was able to be suppressed based on the crystallinity of SiO. In order to decrease the oxygen defect and improve the crystallinity of SiO, Fe_2O_3 was reacted with SiO as an oxygen source then heat-treated at 800 °C. When the sample of the mixed SiO and Fe_2O_3 at a molar ratio of 1:0.2 was heated, Fe_2SiO_4 (fayalite) with the *Pbnm* olivine structure was uniformly formed on the SiO surface. It was confirmed that the efficiency of the first cycle's charge–discharge capacity improved in comparison to the conventional SiO.

1. Introduction

Rechargeable lithium-ion batteries (LIBs) have been used as the power sources for portable digital assistants (e.g., cellular phones, laptop computers and digital cameras) because they have a higher energy density than that of other types of secondary batteries. Alloy type anode materials (i.e., Si [1], Sn [2]) have received considerable attention because of their higher capacity. In particular, silicon (Si) shows the highest theoretical capacity of 4199 mAh g^{-1} ($Li_{22}Si_5$) and low operating potential (vs. Li/Li^+). However, capacity fading occurred during the cycling due to its significantly volume change [3,4]. Silicon monoxide (SiO) can reduce the volume change in Si [5,6], and it shows a better cycle performance than that of Si. SiO is composed of nano-sized Si and amorphous silicon oxides (a-SiO_X) after heat treatment above 900 °C [7–10]. a-SiO_X component in SiO matrix may release the volume expansion of Si and therefore, the cycle performance of SiO can be improved that of Si. However, the first charge–discharge is still a problem as the efficiency of SiO is low [11–13]. The high irreversible capacity is due to the reaction between a-SiO_X and Li. This reaction product is electrochemically inactive against Li, and it is not easy to extract Li from the structure [14,15]. There are few reports using other techniques to improve the reversible capacity, although many researchers have tried to improve the reversibility of the SiO anode material using prelithiation techniques [16].

We reported that this irreversible capacity of SiO occurred between Li and a-SiO_X because the amorphous structure has an oxygen defect and a distortion of the SiO_4 tetrahedral [17]. In this study, we attempted to reduce these structures by experimentally supplying oxygen to SiO by a thermal treatment. However, SiO is oxidized to SiO_2 in the air, thus it is electrochemically inactive against Li [17]. The reaction conditions were then determined in an inert atmosphere. For supplying oxygen to SiO under an inert atmosphere, we have used a redox reaction with the oxide. According to Ellingham

* Corresponding author. Tel.: +81 55 997 9602; fax: +81 55 997 7879.
E-mail address: yamamura@hideyuki.tec.toyota.co.jp (H. Yamamura).

0378-7753/$ – see front matter © 2013 Elsevier B.V. All rights reserved.
http://dx.doi.org/10.1016/j.jpowsour.2013.01.038

diagram, the several oxides can be reduced by Si [18]. In several oxides, we selected Fe_2O_3 because Si has been used as a reducing element due to the refining of Fe_2O_3 in the steel industry [19].

$$2Fe_2O_3 + 3Si \leftrightarrow 4Fe + 3SiO_2 \quad (1)$$

This reaction shows that the oxygen supplies from Fe_2O_3 to Si. Thus, we think that it can reduce the oxygen defects by experimentally supplying oxygen to SiO by a thermal treatment.

2. Experimental methods

Silicon monoxide (SiO, Osaka Titanium Technologies, $D_{50} = 5$ μm) and α-Fe_2O_3 (C. I. Kasei Co., $D_{50} = 39$ nm) were mixed using a planetary ball mill (Premium line P-7, Fritsch) at a molar ratio of 1:0.125. To determine the effect of the reaction temperature, the mixture was thermally treated at 400 °C, 600 °C, 800 °C, and 1000 °C for 3 h in a flowing argon atmosphere. The reaction products were identified by X-ray diffraction (Ultima IV, Rigaku) using CuKα and the scan range was from 10° to 80° at the scan rate of 10° min^{-1}. Since the irreversible capacity was reduced when SiO + Fe_2O_3 was treated at 800 °C, then the molecular ratio of mixture was optimized. The secondary electron images (SEIs) and the backscattered electron images (BEIs) of the reaction product were observed by field-emission scanning electron microscopy (ULTRA55, ZEISS). In addition, cross-section views of reaction products were obtained by scanning transmission electron microscopy (JEM-2100F, JEOL), and the distribution of the atoms was measured by energy-dispersive X-ray spectroscopy.

To observe the electrochemical performance, slurry for the working electrode was prepared by mixing the active material with acetylene black as the electronic conductor and polyimide as the binder in the weight ratio of 75:15:10 in *N*-methylpyrrolidine (NMP) solution. The slurry was then coated on a Cu foil (15 μm in thickness), the prepared electrode was pressed by a role press, and dried. The working electrodes were packed in a 2032-type coin cell (Hohsen Corp.) with the separator, the lithium counter electrode, and the spring that induced a packing pressure on both electrodes to reduce the internal impedance. The electrolyte was 1 M $LiPF_6$ in ethylene carbonate (EC), dimethyl carbonate (DMC) and ethyl–methyl carbonate (EMC) in the volume ratio of 30:40:30, respectively. The half-cells were assembled in an argon-filled glove box and the electrochemical reaction was measured in the voltage range of 0.01–2.5 V (vs. Li/Li^+) at 0.15 mA cm^{-2} current density at 25 °C. The cycle performances were measured within the more practical voltage range of 0.01–1.5 V (vs. Li/Li^+) at 0.75 mA cm^{-2} current density at 25 °C.

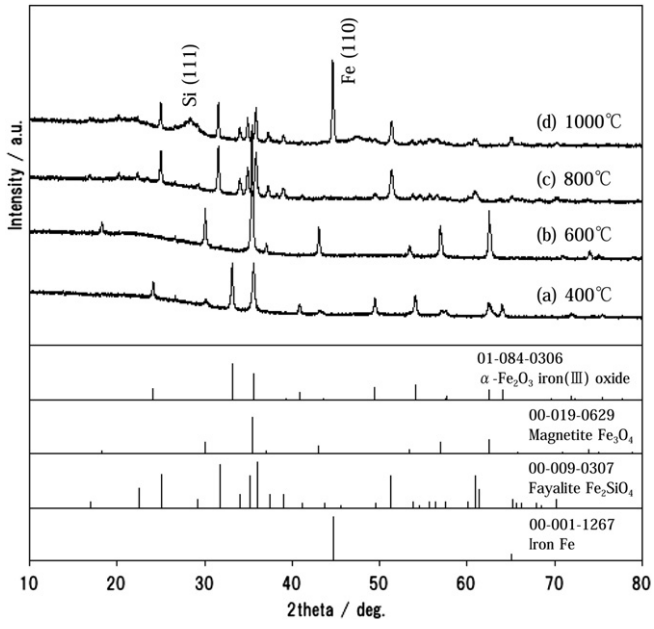

Fig. 1. XRD patterns of the reaction products heated at a molecular ratio of SiO:Fe_2O_3 = 1:0.125 at (a) 400 °C, (b) 600 °C, (c) 800 °C and (d) 1000 °C for 3 h in Ar.

3. Results and discussion

Fig. 1 shows XRD patterns of the reaction products in which the SiO and Fe_2O_3 were at the molecular ratio of 1:0.125 and obtained at four reaction temperatures, i.e., 400 °C, 600 °C, 800 °C and 1000 °C. The oxidation–reduction reaction between SiO and Fe_2O_3 increased in temperature range above 600 °C. For the 600 °C sample, Fe_2O_3 was reduced to Fe_3O_4. For the 800 °C and 1000 °C samples, Fe_2O_3 reduced to Fe_2SiO_4 (Fe^{0+}), which has an olivine structure with a *Pbmn* space group. In addition, clear peaks corresponding to Si (111) and Fe (110) gradually appeared around 28°

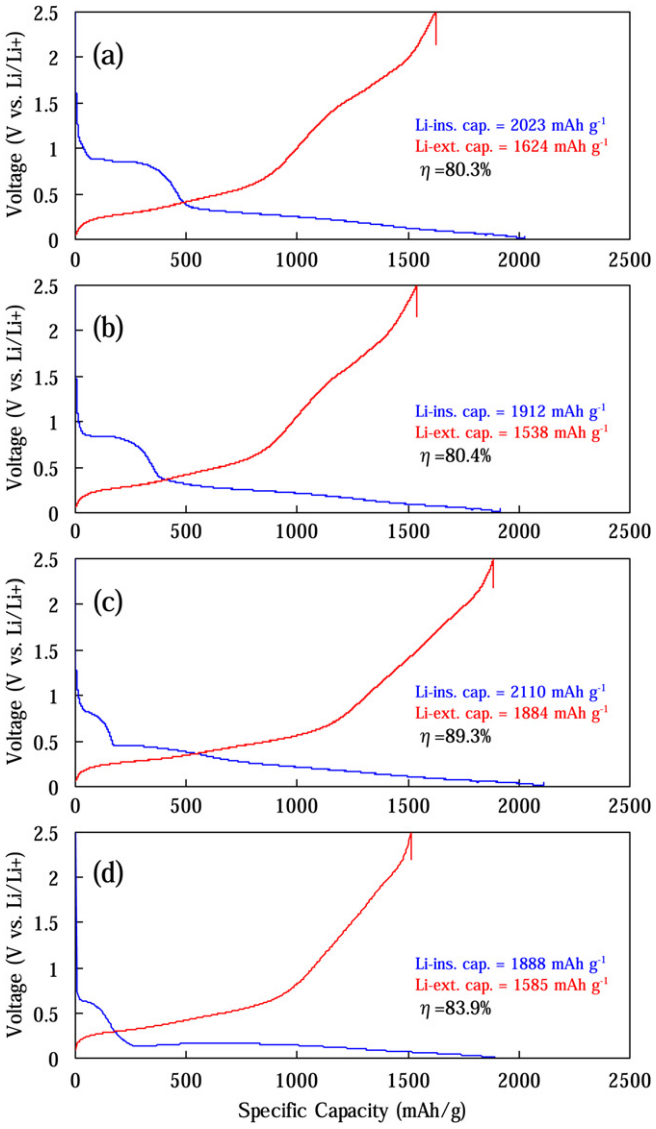

Fig. 2. The charge–discharge profiles of the reaction products heated at a molecular ratio of SiO:Fe_2O_3 = 1:0.125 at (a) 400 °C, (b) 600 °C, (c) 800 °C and (d) 1000 °C for 3 h in Ar.

and 45° for the thermal treated sample at 1000 °C. These results indicated that Fe_2O_3 was reduced by SiO, and oxygen was supplied from Fe_2O_3 to SiO.

Fig. 2 shows the charge–discharge profiles of the heat-treated samples shown in Fig. 1. For 400 °C sample (Fig. 2a), the Li-insertion capacity was 2023 mAh g^{-1} and the Li-extraction capacity was 1624 mAh g^{-1}. For the 600 °C sample (Fig. 2b), the Li-insertion capacity was 1912 mAh g^{-1} and the Li-extraction capacity was 1538 mAh g^{-1}. These curves have a conversion reaction around 1.0 V (vs. Li/Li^+) which was the reaction of the iron oxides and Li [20,21]. The 400 °C sample (Fig. 2a) showed mixed charge–discharge curves of SiO and Fe_2O_3, while the 600 °C sample (Fig. 2b) also showed mixed charge–discharge curves of SiO and Fe_3O_4. When the SiO and Fe_2O_3 were mixed, the calculated Li-insertion capacity was 2031 mAh g^{-1} and the calculated Li-extraction capacity was 1606 mAh g^{-1}. When SiO and Fe_3O_4 were mixed, the calculated Li-insertion capacity was 2062 mAh g^{-1} and the calculated Li-extraction capacity was 1619 mAh g^{-1}. In the case of Fe_3O_4, the charge–discharge capacity was calculated as Fe_2O_3 reduced to Fe_3O_4. These calculated values corresponded to the experimental values. In contrast, the 800 °C sample (Fig. 2c) and the 1000 °C sample (Fig. 2d) also showed a plateau at 1.0 V (vs. Li/Li^+). This plateau indicated that Li can react with Fe_2SiO_4. In addition, the charge–discharge efficiencies of these samples were better than that of the pristine SiO. For the 800 °C sample, the charge–discharge efficiency improved to 89.3% (the Li-insertion capacity was 2110 mAh g^{-1} and the Li-extraction capacity was 1884 mAh g^{-1}) and it showed good reversibility. The charge–discharge efficiency of the 1000 °C sample also improved to 86.4%. When the reaction temperature was 800 °C, the irreversible capacity was the most improved.

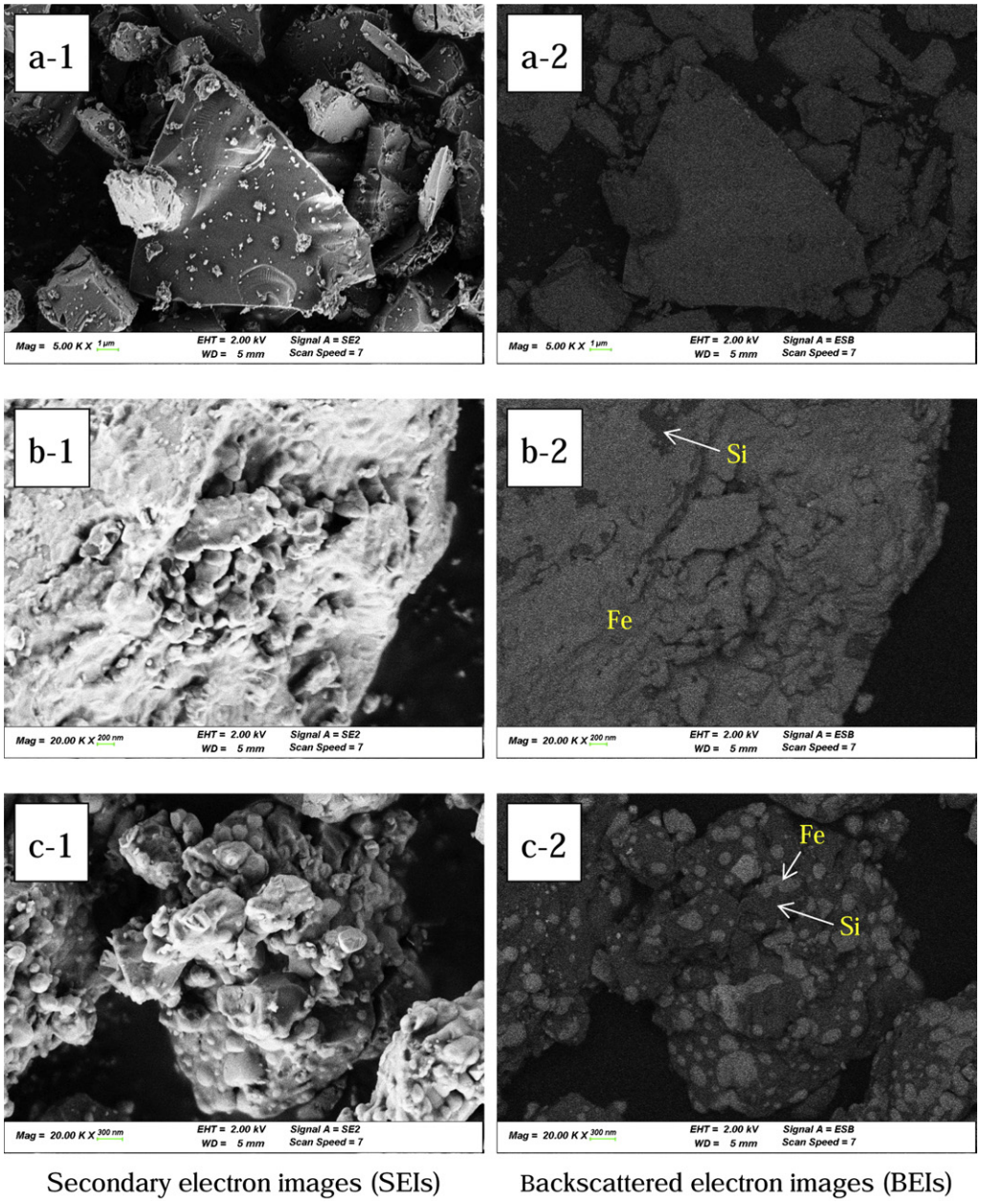

Fig. 3. (a) Secondary electron images and (b) backscattered electron images of (1) SiO and (2) 800 °C sample and (C) 1000 °C sample heated at molecular ratio of $SiO:Fe_2O_3 = 1:0.2$ for 3 h in Ar.

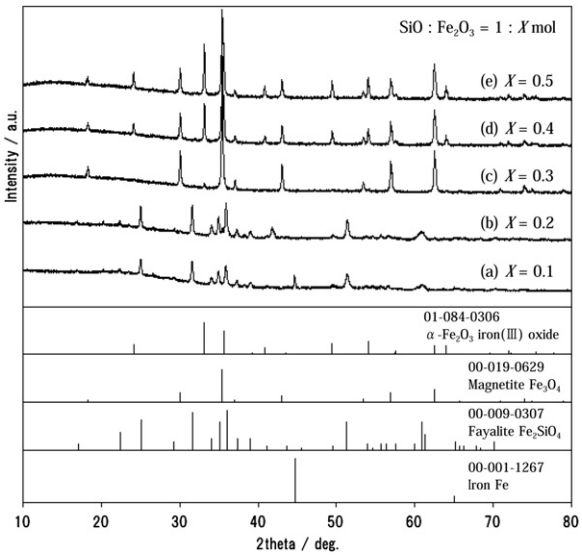

Fig. 4. XRD patterns of SiO:Fe_2O_3 = 1:*X* composites heated at 800 °C for 3 h in Ar. *X* is (a) *X* = 0.1, (b) *X* = 0.2, (c) *X* = 0.3, (d) *X* = 0.4 and (e) *X* = 0.5.

Fig. 3 shows the secondary electron images (SEIs) and the backscattered electron images (BEIs) of (a) SiO, (b) the 800 °C sample and (c) the 1000 °C sample. In the BEIs, the Si atom is shown in the brighter areas and the Fe atom in the darker regions. As depicted in Fig. 3a-1, the surface of SiO is flat and smooth. However, in Fig. 3b-1, which shows the reaction product at 800 °C, the surface morphology differs from that of SiO, and the roughness differs from that observed before heating, and the adhesion of a molten material is seen on the surface. In addition, the surface was uniformly covered by Fe atom, as shown in Fig. 3b-2. The image of the 800 °C sample showed the uniform distribution of the Fe atom. For the 1000 °C sample (Fig. 3c-1), the morphology was similar to the 800 °C sample. However, the Fe element aggregated locally, as shown in Fig. 3c-2. Although to the best of our knowledge, there is no report about the reaction mechanism of SiO and Fe_2O_3, the following may be deduced as the reaction mechanism of SiO_2 and FeO [22,23]. The surface of SiO was oxidized to SiO_2 by reacting with Fe_2O_3, and Fe_2O_3 was reduced to FeO by SiO, and then SiO_2 and FeO reacted to form Fe_2SiO_4 at 800 °C. At 1000 °C, the nano-sized amorphous Si, which is a component of SiO, exhibited a reducing power stronger than that of SiO, and it likely appears that Fe_2O_3 was reduced to Fe by silicon oxides and activated nano-sized Si. Based on these images (Fig. 3) and the charge–discharge efficiency

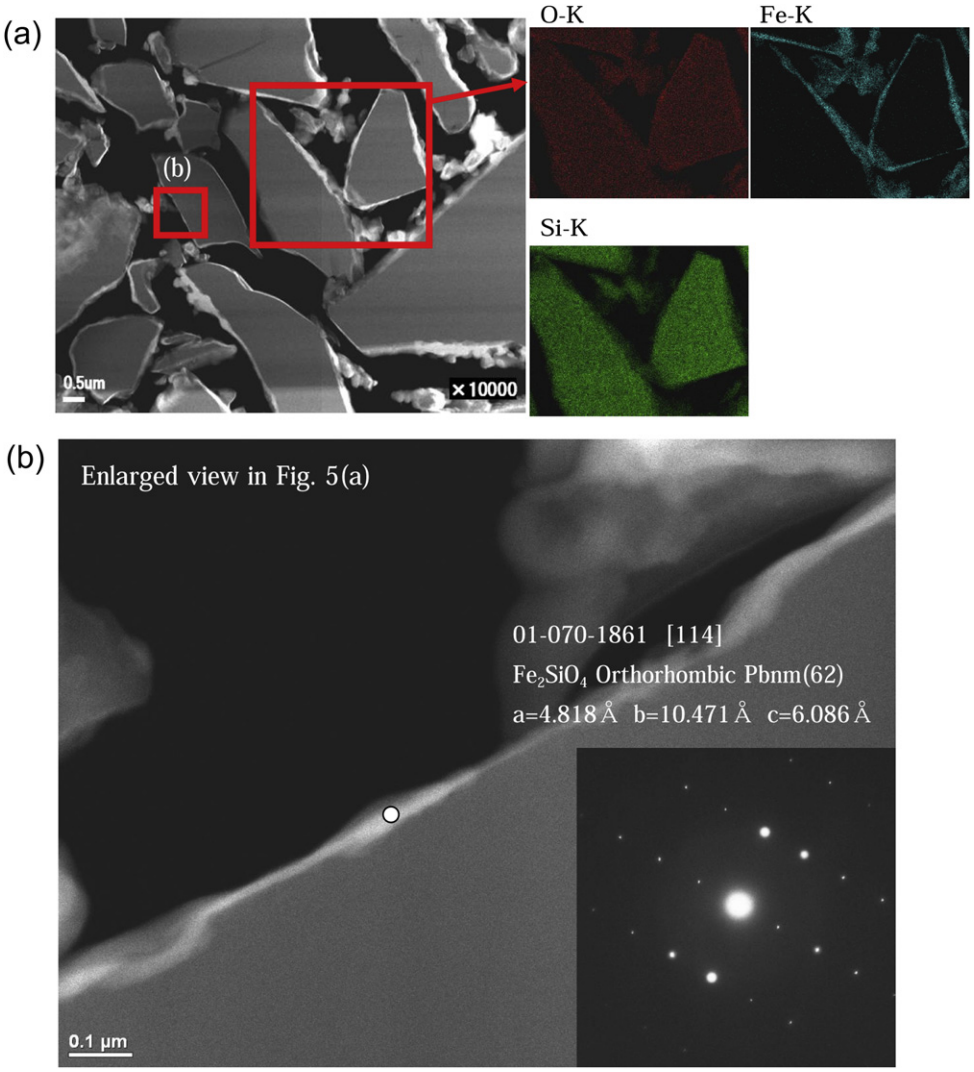

Fig. 5. Cross-section TEM images of SiO + Fe_2O_3 heated at 800 °C at the molecular ratio of SiO:Fe_2O_3 = 1:0.2 for 3 h in Ar. (a) Elemental mapping by EDX and (b) the selected area electron diffraction (SAED) pattern (inset) of the reaction product on the surface of SiO.

(Fig. 2), the reaction temperature was selected 800 °C to react SiO and Fe_2O_3 uniformly, and then the ratio of the oxide mixture X was also optimized.

Fig. 4 shows the XRD patterns of the reaction products obtained by changing a molecular ratio of SiO and Fe_2O_3 at 800 °C. As shown in Fig. 4, the diffraction patterns were classified into the following three categories: $X \leqq 0.2$, $X = 0.3$ and $X \geqq 0.4$. For $X \leqq 0.2$, the diffraction pattern indicated Fe_2SiO_4. For $X = 0.3$, Fe_2O_3 was reduced to Fe_3O_4. For $X \geqq 0.4$, Fe_2O_3 was not reduced, but was instead maintained. The best composition of SiO and Fe_2O_3 was identified as SiO:Fe_2O_3 = 1:0.2 mol.% from XRD pattern and the first cycle's charge–discharge efficiency (Fig. 3).

The cross-section images of SiO + Fe_2O_3, which were synthesized at the molecular of SiO:Fe_2O_3 = 1:0.2 for 3 h at 800 °C under an argon atmosphere observed by TEM and the distribution of atoms measured by EDX, are shown in Fig. 5. In Fig. 5a, the thickness of the reaction layer was 50–100 nm and the reaction product was deposited on the SiO surface. From the element mapping by EDX, Fe did not diffuse into SiO matrix, but reacted on the surface only. Based on the selected area electron diffraction (SAED) results, the reaction product on the surface should certainly be orthorhombic Fe_2SiO_4. These results suggest that Fe_2SiO_4 (see the XRD in Figs. 1, 4 and 5) was formed on the SiO surface, and the Fe element did not influence the SiO bulk. As Fe_2SiO_4 exists on the surface, the electric conductivity of this powder improved from 10^{12} S cm^{-1} to 10^{10} S cm^{-1}, and the surface area was increased from 2.45 m^2 g^{-1} to 3.65 m^2 g^{-1} after heating.

Fig. 6 shows the charge–discharge curves of (a) heat-treated SiO at 800 °C, and (b) SiO + Fe_2O_3 for 3 h at 800 °C. In Fig. 6a, the anodic performance of the heat-treated SiO was as follows: the Li-insertion capacity was 2615 mAh g^{-1}, the Li-extraction capacity was 1824 mAh g^{-1}, and the efficiency of the charge–discharge capacity was 69.8%. This result corresponded with the reported capacity and the efficiency of the charge–discharge capacity [6]. In contrast, as shown in Fig. 6b, the anodic performance of SiO + Fe_2O_3 showed a vast improvement in reversibility, such that the Li-insertion

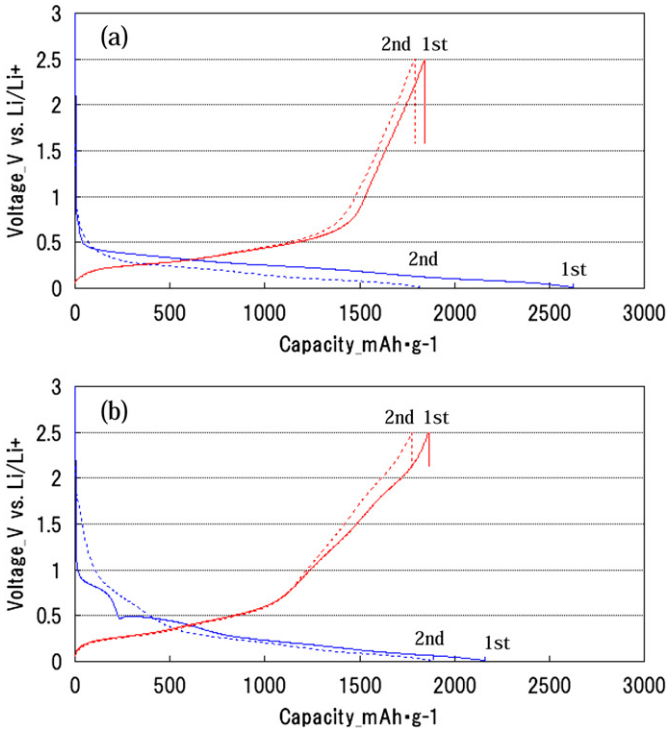

Fig. 6. The charge–discharge curves of (a) heated SiO at 800 °C and (b) SiO + Fe_2O_3.

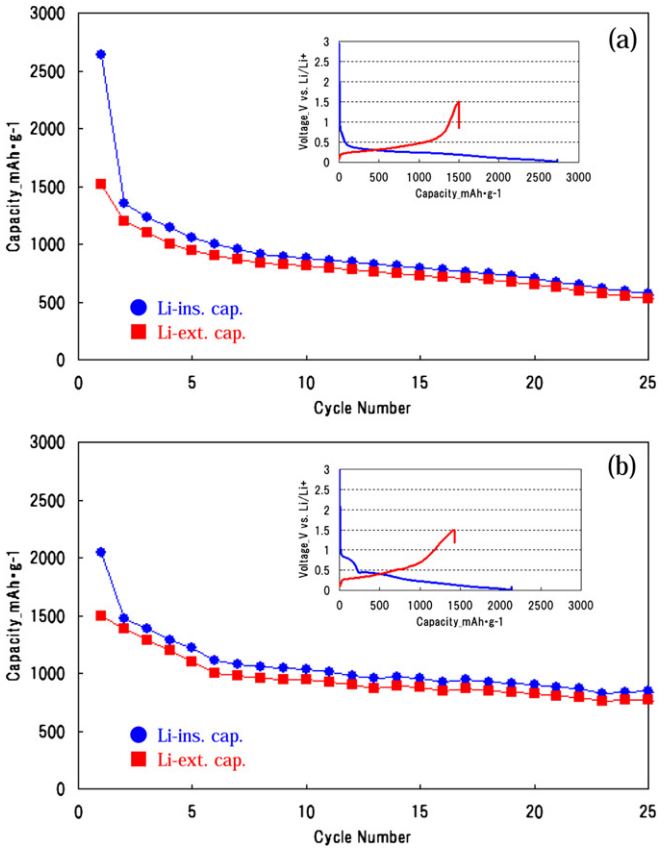

Fig. 7. The cycle performance of (a) heated SiO at 800 °C and (b) SiO + Fe_2O_3.

capacity was 2095 mAh g^{-1}, the Li-extraction capacity was 1900 mAh g^{-1}, and the efficiency of the charge–discharge capacity was 90.6%. We concluded that the fading of the Li-insertion capacity was due to decrease in Si as the active material by reacting with Fe_2O_3. However, this reversibility was improved by over 10% in comparison to the conventional SiO, and it also showed good cycle reversibility in Fig. 7. The charge–discharge curve of SiO + Fe_2O_3 differed from that of SiO. For the Li-insertion process of SiO + Fe_2O_3, the plateau at 0.5 V (vs. Li/Li$^+$) in Fig. 6b indicates that Li ion reacted with Fe_2SiO_4 (the same reaction as in Fig. 2). For the Li-extraction process, there was no difference in the profiles of SiO and SiO + Fe_2O_3 in the voltage range below 0.6 V (vs. Li/Li$^+$). However, the Li-extraction profile differed in the voltage range above 0.6 V (vs. Li/Li$^+$). Regarding the Li-extraction process, it has been reported that Li ion could extracted from the Li–Si alloy and the reaction product, which was formed by the reaction of a-SiO_X with Li, could be electrochemically inactive. As you can see in Fig. 6b, the slope of the profile in the voltage range above 0.6 V (vs. Li/Li$^+$) is gradual, and thus our results indicate that Li ion was extracted from the reaction product which had been thought to be electrochemically inactive. Although the irreversible capacity was improved by the reaction of SiO and Fe_2O_3, it is thought that the lithium–silicate forming reaction of a-SiO_X and Li was not inhibited because the SiO bulk did not change after heating. Therefore, we postulated that the surface modification by the Fe_2SiO_4 layer was one of the factors influencing the improvement of the reversibility.

4. Conclusions

To reduce the irreversible capacity of SiO anode material at the first cycle, Fe_2O_3 reacted with SiO for 3 h at 800 °C under an argon atmosphere. When the molecular ratio of SiO:Fe_2O_3 = 1:0.2,

Fe_2SiO_4 was only formed on the SiO surface. The thickness of this layer was 50–100 nm, and it uniformly formed. The anodic performance of SiO + Fe_2O_3 material showed that the Li-insertion capacity was 2095 mAh g^{-1}, the Li-extraction capacity was 1900 mAh g^{-1} and the charge–discharge efficiency had significantly improved from 70% to 90%. However, these results indicate that an improved reversibility for the SiO anode can be achieved, and it is expected that this finding will make a breakthrough in the study and uses of the SiO anode-active material.

References

[1] J.R. Dahn, T. Zheng, Y. Liu, J.S. Xue, Science 270 (1995) 590–598.
[2] M. Winter, J.O. Besenhard, Electrochim. Acta 45 (1999) 31–50.
[3] W.R. Lin, Z.A. Guo, W.S. Young, D.T. Shieh, H.C. Wu, M.H. Yang, N.L. Wu, J. Power Sources 140 (2005) 139–144.
[4] N. Dong, J. Xu, Y. Yao, G. Wegner, I. Lieberwirth, C. Chen, J. Power Sources 192 (2009) 644–651.
[5] T. Morita, N. Takami, J. Electrochem. Soc. 153 (2) (2006) A425–A430.
[6] M. Yamada, A. Inaba S. Nagayama, K. Matsumoto, A. Ueda and, T. Ohzuku, "The 50th Battery Symposium in Japan", Nov. 30–Dec. 2, Kyoto, Japan, (2009) 2C12.
[7] A. Hohl, T. wieder, P.A. van Aken, T.E. Weirich, G. Denninger, M. Vidal, S. Oswald, C. Deneke, J. Mayer, H. Fuess, J. Non-Cryst. Solids 320 (2003) 255–280.
[8] M. Mamiya, H. Takei, M. Kikuchi, C. Uyeda, J. Cryst. Growth 229 (2001) 457–461.
[9] M. Mamiya, M. Kikuchi, H. Takei, J. Cryst. Growth 237–239 (2002) 1909–1914.
[10] Y. Nagao, H. Sakaguchi, H. Honda, T. Fukunaga, T. Esaka, J. Electrochem. Soc. 151 (10) (2004) A1572–A1575.
[11] J. Yang, Y. Takeda, N. Imanishi, C. Capiglia, J.Y. Xie, O. Yamamoto, Solid State Ionics 152–153 (2002) 125–129.
[12] T. Tabuchi, H. Yasuda, M. Yamachi, J. Power Sources 146 (2005) 507–509.
[13] Y. Li, Z.Y. Wen, X.Y. Wang, X.L. Yang, A. Hirano, N. Imanishi, Y. Takeda, J. Power Sources 189 (2009) 480–484.
[14] M. Miyachi, H. Yamamoto, H. Kawai, T. Ohta, M. Shirakata, J. Electrochem. Soc. 152 (10) (2005) A2089–A2091.
[15] M. Miyachi, H. Yamamoto, H. Kawai, J. Electrochem. Soc. 154 (4) (2007) A376–A380.
[16] T. Miyuki, Y. Okuyama, T. Sakamoto, Y. Eda, T. Kojima, T. Sakai, Electrochem. Soc. Jpn. 80 (6) (2012) 401–404 [in Japanese].
[17] H. Yamamura, K. Nobuhara, S. Nakanishi, H. Iba, J. Ceram. Soc. Jpn. 119 (11) (2011) 855–860.
[18] H.T.T. Ellingham, J. Soc. Chem. Ind. (London) 63 (1944) 125.
[19] R. Seshadria, Met. Mat. Proc. 12 (2–3) (2000) 223–240.
[20] H. Liu, G. Wang, J. Park, J. Wang, H. Liu, C. Zhang, Electrochim. Acta 54 (2009) 1733–1736.
[21] Q. Zhang, Z. Shi, Y. Deng, J. Zheng, G. Liu, G. Chen, J. Power Sources 197 (2012) 305–309.
[22] A. Nakamura, H. Schmalzried, Phys. Chem. Miner. 10 (1983) 27–37.
[23] A.S. Arico, P. Bruce, B. Scrosati, J.-M. Tarascon, W.V. Schalkwijk, Nat. Mater. 4 (2005) 366–377.